Original Article

OXPAT/PAT-1 Is a PPAR-Induced Lipid Droplet Protein That Promotes Fatty Acid Utilization

Nathan E. Wolins,[1] Benjamin K. Quaynor,[1] James R. Skinner,[1] Anatoly Tzekov,[1] Michelle A. Croce,[2] Matthew C. Gropler,[2] Vijayalakshmi Varma,[3] Aiwei Yao-Borengasser,[3] Neda Rasouli,[3] Philip A. Kern,[3] Brian N. Finck,[2] and Perry E. Bickel[1,4]

Lipid droplet proteins of the PAT (perilipin, adipophilin, and TIP47) family regulate cellular neutral lipid stores. We have studied a new member of this family, PAT-1, and found that it is expressed in highly oxidative tissues. We refer to this protein as "OXPAT." Physiologic lipid loading of mouse liver by fasting enriches OXPAT in the lipid droplet tissue fraction. OXPAT resides on lipid droplets with the PAT protein adipophilin in primary cardiomyocytes. Ectopic expression of OXPAT promotes fatty acid–induced triacylglycerol accumulation, long-chain fatty acid oxidation, and mRNAs associated with oxidative metabolism. Consistent with these observations, OXPAT is induced in mouse adipose tissue, striated muscle, and liver by physiological (fasting), pathophysiological (insulin deficiency), pharmacological (peroxisome proliferator–activated receptor [PPAR] agonists), and genetic (muscle-specific PPARα overexpression) perturbations that increase fatty acid utilization. In humans with impaired glucose tolerance, PPARγ agonist treatment induces adipose OXPAT mRNA. Further, adipose OXPAT mRNA negatively correlates with BMI in nondiabetic humans. Our collective data in cells, mice, and humans suggest that OXPAT is a marker for PPAR activation and fatty acid oxidation. OXPAT likely contributes to adaptive responses to the fatty acid burden that accompanies fasting, insulin deficiency, and overnutrition, responses that are defective in obesity and type 2 diabetes. *Diabetes* 55:3418–3428, 2006

From the [1]Division of Endocrinology, Metabolism, and Lipid Research, Department of Medicine, Washington University School of Medicine, St. Louis, Missouri; the [2]Division of Geriatrics and Nutritional Science, Department of Medicine, Washington University School of Medicine, St. Louis, Missouri; the [3]Division of Endocrinology, Central Arkansas Veterans Healthcare System and University of Arkansas for Medical Sciences, Little Rock, Arkansas; and the [4]Department of Cell Biology and Physiology, Washington University School of Medicine, St. Louis, Missouri.

Address correspondence and reprint requests to Perry E. Bickel, Departments of Medicine and of Cell Biology and Physiology, 660 S. Euclid Ave., Campus Box 8127, St. Louis, MO 63110. E-mail: pbickel@im.wustl.edu.

Received for publication 24 March 2006 and accepted in revised form 6 September 2006.

Additional information for this article can be found in an online appendix at http://diabetes.diabetesjournals.org.

Acadm, medium-chain acyl-CoA dehydrogenase; Acadv1, very-long-chain acyl-CoA dehydrogenase; BAT, brown adipose tissue; Cox4, cytochrome C oxidase 4; EST, expressed sequence tag; IBMX, 3-isobutyl-1-methylxanthine; LCFA, long-chain fatty acid; PAT, perilipin, adipophilin, and TIP47; PPAR, peroxisome proliferator–activated receptor; Sdha, subunit a of succinate dehydrogenase; STZ, streptozotocin; TAG, triacylglycerol; TZD, thiazolidinedione; WAT, white adipose tissue.

DOI: 10.2337/db06-0399

Most mammalian cells have the capacity to store fatty acids as triacylglycerol (TAG) for subsequent use as substrates for membrane synthesis, ATP production, and gene regulation. How and to what extent cells and tissues store, mobilize, and utilize fatty acids is influenced by the family of PAT (perilipin, adipophilin, and TIP47) proteins (1–5), which share regions of sequence similarity and a propensity to coat lipid droplets. As components of the lipid droplet coat, PAT proteins lie at the interface between the neutral lipid core and the aqueous cytosol, and therefore are positioned to regulate lipid storage and mobilization. This control over cellular lipid has proved important in whole-organism energy homeostasis (6–8).

Five potential mammalian PAT family members were reported when the family was defined (1). Protein products for four of the five mammalian genes in this family have been characterized and shown to bind lipid droplets (9–13). These proteins likely are synthesized in the cytosol and bind lipid droplets posttranslationally (14,15). Perilipin and adipophilin are stable only in the presence of neutral lipid and, otherwise, are targeted to proteosomes for degradation (16,17). Perilipin and adipophilin are necessary for accumulation of large TAG stores in adipose tissue (7,8) and liver (6), respectively, and likely are important for regulation of constitutive TAG stores. Also, evidence has amassed that perilipin regulates and orchestrates the hydrolysis of adipose TAG stores (2,4,5,7,8). In contrast, TIP47 and S3-12 are stable in the absence of neutral lipid and are found in the cytosol when ambient lipid levels are low. For most cultured cells, when standard lean media are supplemented with long-chain fatty acid (LCFA), nascent TIP47-coated TAG droplets emerge; in adipocytes, droplets emerge coated with both TIP47 and S3-12 (9,10,18) that are recruited from a preexisting cytosolic pool. TIP47 and S3-12 likely serve as a reserve of exchangeable lipid droplet coat necessary for rapid TAG storage (18). A fifth PAT protein, PAT-1, was discussed in the article that defined the family (1), but the cDNA and protein sequences for this protein were not reported.

Genomic sequences and expressed sequence tags (ESTs) from several species that are similar but not identical to the known PAT proteins have been deposited in GenBank (19). Based on these sequences and the prior report of a fifth PAT protein, we deduced the existence of an uncharacterized PAT protein. We obtained a full-length mouse cDNA that corresponded to these genomic and EST sequences and raised antibodies against the predicted

protein. We have found that this protein is most highly expressed in tissues that catabolize large amounts of fatty acids, is upregulated by treatments that increase fatty acid utilization, promotes both TAG storage and fatty acid oxidation when ectopically expressed in cells, and coats lipid droplets during rapid TAG synthesis. Further, the relevance of this novel PAT protein to human lipid metabolism is suggested by its regulation in adipose tissue by peroxisome proliferator–activated receptor (PPAR)-γ activation and its negative correlation with BMI in nondiabetic humans. The association of this protein with oxidative metabolism and its similarity to other PAT proteins have led us to name it OXPAT.

RESEARCH DESIGN AND METHODS

Identification of OXPAT. Query of GenBank with TIP47 revealed a mouse cDNA sequence similar to but distinct from the previously characterized PAT proteins (19). This sequence in the expression vector pCMV-SPORT6 (Invitrogen, Carlsbad, CA) was purchased from Open Biosystems (clone ID 5136320). Sequencing of pCMV-SPORT6-OXPAT revealed a full-length cDNA identical to NCBI accession no. AK075872.

PAT proteins sequence alignment. Protein alignments of OXPAT with mouse adipophilin (NM_007408) and mouse TIP47 (NM_007408) utilized Align X in the Vector NTI program (Invitrogen).

Mouse studies. Adult male C57BL/6 mice were utilized. Mice with generalized PPARα deficiency (PPARα KO mice) or muscle-specific PPARα overexpression (MCK-PPARα) have been previously described (20–22) and were extensively backcrossed into the C57BL/6 background. For high-fat diet studies, mice were given ad libitum access to chow providing 43% of its energy as long-chain triglycerides (21) for 12 weeks before they were killed. Ligands for PPARα (Wy-14643; 0.1% wt/wt) or PPARγ (rosiglitazone; 0.06% wt/wt) were incorporated into standard rodent chow (Diet 5053; Purina Mills, St. Louis, MO), and mice were given ad libitum access to PPAR ligand–containing chow for 1 week before they were killed.

For fasting studies, mice were separated into individual cages at the beginning of each experiment. Fasting was initiated at 0800 and mice were fasted for 24 h. Control mice were allowed ad libitum access to standard rodent chow. Insulin deficiency was induced by a single intraperitoneal injection of streptozotocin (STZ; 180 mg/kg body wt; Sigma Chemical) and was confirmed 3 days postinjection by tail blood glucose monitoring (B-GLUCOSE Analyzer; Hemacue AB, Angelholm, Sweden). Mice with blood glucose of >400 mg/dl were considered insulin deficient and were killed 7 days after STZ injection. All animal experiments were approved by the Animal Studies Committee of Washington University School of Medicine.

Northern blotting of mouse tissues. Total cellular RNA was isolated and Northern blot analyses performed as previously described (23).

Protein extraction from tissues and immunoblotting. For the tissue immunoblot in Fig. 2*B*, tissues were harvested from a 22-g, 8-week-old, male C57BL/6 mouse. For all immunoblots, proteins were extracted (10) and immunoblotted (18) as described previously. Lanes were equally loaded for protein (30 μg/lane) on all immunoblots, except for the cell/tissue fractionation blots, in which lanes were loaded with equal proportions of each fraction.

Antibodies. Proteintech (Chicago, IL) generated the following antisera by injecting the following keyhole limpet hemocyanin-conjugated peptides into rabbits: MDQRGEDTTLAPHSRMSGDC, which corresponds to the NH_2-terminus of OXPAT (α-N-OXPAT); EAEPPRGQGKHTMMPELDFC, which corresponds to the COOH-terminus of OXPAT (α-OXPAT-C) (see Fig. 1); and GPFAPGITEKTPEGKC, which corresponds to the COOH-terminus of TIP47 (α-TIP47-C). Antibodies were purified from antiserum using the immobilized immunizing peptide. Peptide immobilization, antibody binding, and elution were done as recommended by the manufacturer (Pierce, catalog no. 44895). The rabbit antibodies against the NH_2-termini of mouse S3-12 (α-N-S3-12) (10) and mouse TIP47 (α-N-TIP47) (18) have been described previously. The guinea pig antisera against mouse adipophilin (18) and perilipin (24) were purchased from Fitzgerald Industries International (Concord, MA; catalog nos. RDI-PROGP40 and RDI-PROGP29, respectively). Mouse monoclonal antibodies against caveolin-2 and calnexin were purchased from BD Biosciences (San Jose, CA; catalog no. 610684 and 610523, respectively). Mouse monoclonal antibodies against adipophilin were purchased from American Research Products (Belmont, MA; catalog no. 03-651102).

Tissue culture. COS-7 (18) and OP9 (25) cells lines were cultured as previously described.

Construction of OXPAT and S3-12 expression constructs. To generate OXPAT expression vectors with Kozak sequences and without OXPAT untranslated sequence, the following oligonucleotides were used as primers in a PCR: forward primer TCTGGTGTGCGGGTCTGTCCCTAC and reverse primer GCGGCCGCGTCACATGACCACCAGGGGGC. To attach a myc-epitope to the NH_2-terminus of OXPAT, the following forward primer was used in a PCR with the reverse primer described above: GAAGATCTACCATGGAGCAGAAACTC ATCTCTGGTGAAGAGGATCTGATGGACCAGAGAGGTGAAGACACC. pCMV-SPORT6-OXPAT was used as the template. The resulting PCR product was TA cloned into pcDNA3.1/V5-His-TOPO according to the manufacturer's recommendations (Invitrogen, Carlsbad, CA). The coding regions of these constructs were subcloned into the Δ U3 retroviral vector (26).

Generation of stable cell lines. To generate pseudotyped retroviral particles, the Δ U3 vector with the appropriate insert was transfected into 293 GPG cells (26). These viral particles were used to make the following stable cell lines: COS 7 cells expressing myc-OXPAT-A (COS-7 myc-OXPAT-A), COS-7 cells expressing LacZ with a nuclear localization sequence (COS-7 LacZ), OP9 cells expressing OXPAT (OP9 OXPAT), and OP9 cells expressing NLS-LacZ (OP9-LacZ).

Liver fractionation. Livers from 11-week-old fed and fasted male C57BL/6 mice were homogenized by three strokes in a motor-driven Teflon pestle tissue homogenizer. The 2,000*g* × 5 min supernatant was weighted to 45% (wt/wt) sucrose with 70% sucrose in lysis buffer (10 mmol/l HEPES, 1 mmol/l EDTA, pH 7.3). In centrifuge tubes, the sucrose-weighted liver extracts were overlaid with successive layers of 1 ml 40% sucrose and 1 ml 10% sucrose. The tubes were then filled to the 5-ml capacity with lysis buffer. The gradients were centrifuged at increasing forces as follows: 5 min at 2,700*g*, 10 min at 10,700*g*, 20 min at 43,000*g*, and 30 min at 172,000*g* and then allowed to coast to a stop. Fractions were harvested as described previously (18).

Adult mouse cardiomyocyte isolation. The heart from an 18-week-old male C57BL/6 mouse was harvested and cardiomyocytes isolated and plated onto coverslips as previously described (27).

TAG measurements. Since the gradient fractions were from well-disrupted cells, these fractions were added directly to the colorimetric TAG quantification reagent (10). To make the TAG in intact cells accessible, the TAG was solvent extracted before colorimetric quantification (25).

Immunofluorescence microscopy. Imaging of COS-7 myc-OXPAT-A cells and adult mouse cardiomyocytes was performed as described previously (10).

Palmitate oxidation assays. COS-7 or OP9 cells stably transduced with OXPAT or LacZ (control) were plated in 24-well culture dishes. Twenty-four hours after plating, palmitate oxidation rates were determined using [9,10-^{3}H]palmitic acid as previously described (28). Rates were corrected for cellular protein and normalized (= 1.0) to LacZ values.

TAG accumulation assay. Oleate complexed to albumin in a 5.5:1 molar ratio was added to culture media from an 18 mmol/l stock to a final concentration of 1 mmol/l. At the times indicated, cells were dispersed. Aliquots of dispersed cells were then used to measure protein and were solvent extracted before TAG measurement.

Mouse muscle histology. Gastrocnemius muscle from high fat–fed MCK-PPARα and nontransgenic control mice were frozen in Optimal Cutting Temperature compound (Sakura Finetech, Torrance, CA), sectioned, stained with α-OXPAT-C (400 ng/ml), and visualized using fluorescently labeled secondary antibodies.

Human subjects. Healthy weight-stable subjects without diabetes were recruited and provided written, informed consent under protocols that were approved by the local institutional review board, and studies were conducted at the University of Arkansas for Medical Sciences General Clinical Research Center. Subjects were receiving no drugs likely to affect adipose tissue or lipid metabolism, such as fibrates, ACE inhibitors, or angiotensin II receptor blockers. Based on an initial 75-g oral glucose tolerance test, subjects were defined as either normal glucose tolerant (NGT; fasting blood glucose <110 mg/dl, 2-h glucose <140 mg/dl) or impaired glucose tolerant (IGT; 2-h glucose 140–199 mg/dl). Eighty-five subjects were included in this study, of which 69 were women, 16 were men, 46 were NGT, and 39 were IGT, and the age range was 21–66 years old. Subcutaneous adipose tissue and muscle biopsies were performed, along with insulin sensitivity testing, and IGT subjects were then randomized to receive either metformin or pioglitazone for 10 weeks, as described previously (29), after which the studies were repeated. Insulin sensitivity was measured by an insulin-modified frequently sampled intravenous glucose tolerance test using 11.4 g/m^2 of glucose and 0.04 units/kg of insulin, as described previously (30). Plasma insulin and glucose were measured as described (29), and insulin sensitivity was calculated using the MINMOD Millennium program (31).

RNA isolation and real-time RT-PCR. Real-time quantitative RT-PCR was performed on cultured cells and mouse tissues as previously described (21). Arbitrary units of target mRNA were corrected to levels of 36B4

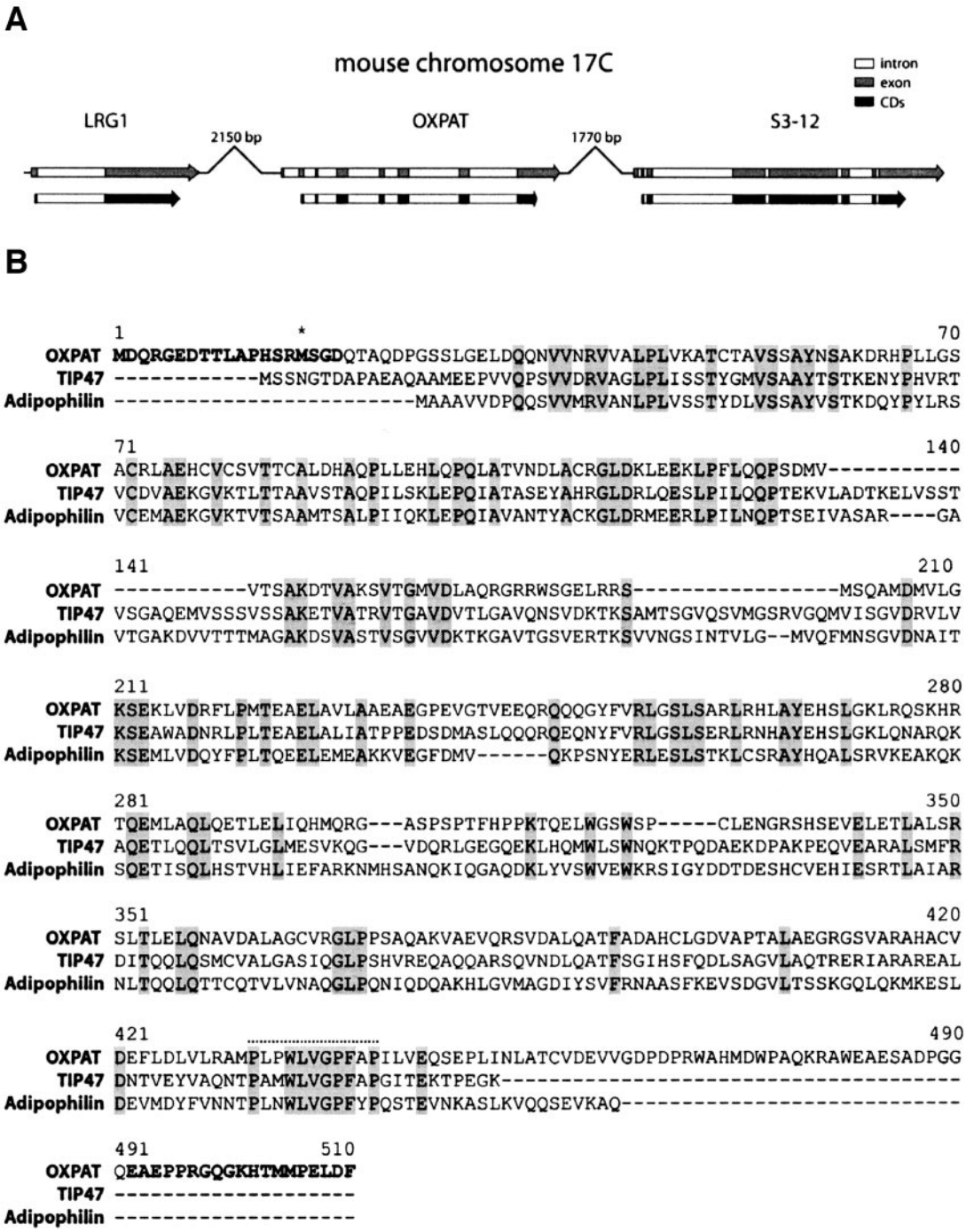

FIG. 1. Position of OXPAT in the mouse genome and OXPAT alignment with TIP47 and adipophilin. *A*: *Oxpat* gene structure and the surrounding region of mouse chromosome 17C are depicted. The relative distances between the genes are noted. *B*: The amino acid sequences of mouse OXPAT, TIP47, and adipophilin are aligned. Bold type indicates the NH_2- and COOH-terminal epitopes against which we raised α-N-OXPAT and α-OXPAT-C antibodies, respectively. Shaded residues are identical among the three sequences at those positions. The asterisk indicates a reported translation start site for PAT-1 (1) (GenBank accession no. AY919875).

mRNA. Total RNA from human adipose tissue and muscle biopsies was isolated and used as template for real-time RT-PCR as previously described (32). The quantity and quality of the isolated RNA were determined by Agilent 2100 Bioanalyser (Palo Alto, CA). All data were expressed in relation to 18S RNA, where the standard curves were generated using pooled RNA from the samples assayed. The primer sequences used for gene expression analysis in mouse and human tissues are provided in supplementary Tables 1 and 2, which are available as online appendixes at http://diabetes.diabetesjournals.org.

Statistics. Student's two-sample *t* tests were used to compare groups, and paired *t* tests were used to compare baseline and posttreatment values within a group. Pearson's correlation coefficients were used to describe the linear association between variables. For each of these analyses, distributional assumptions were evaluated and natural log transformations were applied as necessary. Results based on analyses requiring transformations are noted. All data from human samples are expressed as means ± SEM.

RESULTS

Database identification of OXPAT. We sought to detect novel members of the PAT family by targeted database searches. These searches revealed a cDNA sequence with a conceptual translation homologous to PAT proteins

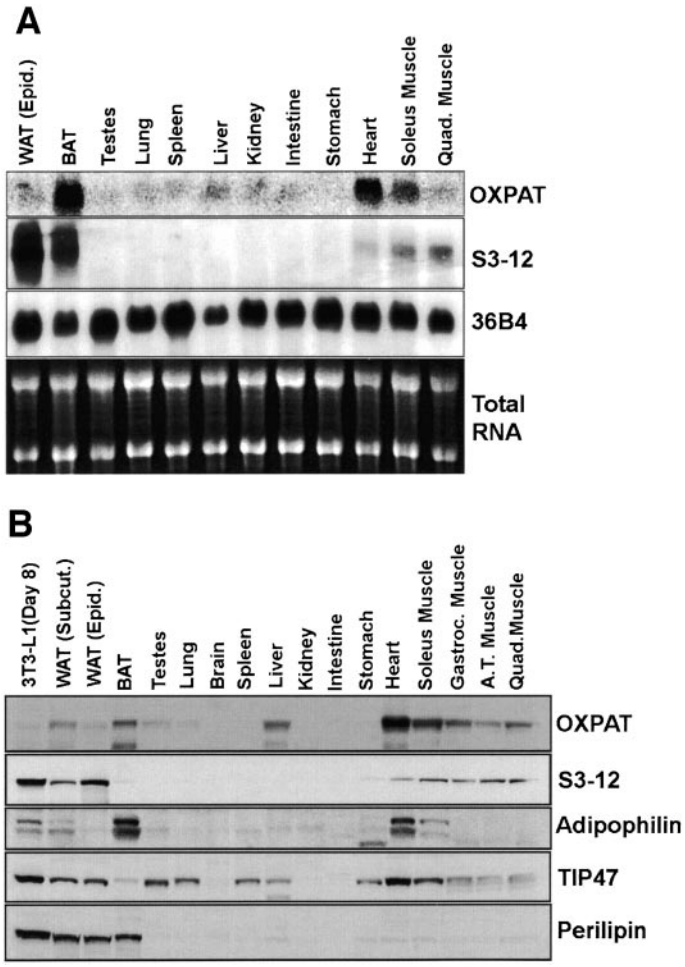

FIG. 2. OXPAT is expressed in tissues with high oxidative capacity. *A*: Mouse tissues were analyzed by Northern blot. Each lane contained 15 μg pooled RNA isolated from male C57BL/6 mice. The blot was sequentially hybridized with radiolabeled cDNA probes for OXPAT, S3-12, and 36B4. *B*: Proteins extracted from 3T3-L1 adipocytes and from the indicated mouse tissues were immunoblotted (30 μg protein per lane) and proteins detected with specific antibodies or antisera at the following concentrations: α-OXPAT-C 400 ng/ml, α-N-TIP47 320 ng/ml, guinea pig antiserum against mouse adipophilin diluted 1:750, α-N-S3-12 800 ng/ml, and guinea pig antiserum against perilipin diluted 1:5,000.

(NCBI accession no. AK075872). This cDNA sequence also has been deposited with the name PAT-1 (1) (accession no. AY919875). Based on the results of our characterization of the protein product of these sequences, we refer to the protein as OXPAT. The gene encoding OXPAT is found on mouse chromosome 17C juxtaposed between the *Lrg1* and *S3-12* genes (Fig. 1*A*). In addition, the gene encoding TIP47 is also found on chromosome 17 within 200 kbp of the *Oxpat* gene. The human gene for OXPAT resides on chromosome 19 (19 p13.3) and, as in the mouse, lies immediately upstream of the *S3-12* gene. The deduced sequence of mouse OXPAT protein is encoded in seven exons flanked by one upstream noncoding exon. OXPAT is a hydrophilic, slightly acidic protein of 463 amino acids with a predicted molecular weight of 51.4 kDa. No intracellular targeting motifs (33,34), other than its similarity to other lipid droplet proteins, were detected (35) (Pfam accession no. PF03036).

The predicted amino acid sequence of mouse OXPAT is 30% identical and 41.4% similar to TIP47 and is 25.6% identical and 38.1% similar to adipophilin. Differences in size and structure between OXPAT and S3-12 and perilipin limit sequence identity and similarity to specific domains. For example, OXPAT, TIP47, adipophilin, and S3-12 all share the PLxWLGFPxxP motif (36) near the COOH-termini. Also, OXPAT is 41.6% identical and 57.4% similar to perilipin within the first 100 amino-terminal residues. OXPAT, like other PAT proteins, lacks long runs of hydrophobic residues that would correspond to a signal peptide or transmembrane domains. These data suggest that OXPAT, like the other PAT proteins, is not directed into the secretory pathway (9,14,15).

The OXPAT protein is longer than TIP47 and adipophilin, leaving unique overhanging sequence at both termini. We raised antipeptide antibodies to epitopes within the unique termini of OXPAT. Both antibodies (α-N-OXPAT and α-OXPAT-C) precipitate OXPAT and recognize SDS-PAGE–resolved OXPAT by immunoblot (supplemental Fig. 1). We have confirmed that neither antibody recognizes an epitope of OXPAT that is exposed on the surface of intact cells (supplemental Fig. 2).

As noted above, an mRNA sequence identical to OXPAT termed PAT-1 has been deposited recently in GenBank. The predicted start methionine for PAT-1 corresponds to the internal methionine at position 16 in the OXPAT protein sequence shown in Fig. 1*B*. Residues 1–15 in the OXPAT sequence are encoded within exon 2 of the *Oxpat* gene. Although OXPAT proteins that start with either methionine could be generated by alternative splicing or by using different translation start sites within the same transcript, we have determined experimentally that the predominant OXPAT protein expressed in mouse tissues begins with the methionine at position 1 (supplemental Figs. 1*B* and 3). We refer to the longer, more abundant isoform as OXPAT-A and the slightly shorter, less abundant isoform as OXPAT-B. OXPAT-A is recognized by both the NH_2- and COOH-terminal OXPAT antibodies, but OXPAT-B is only recognized by α-OXPAT-C (supplemental Fig. 3).

OXPAT expression is enriched in tissues with high oxidative capacity. To define the tissues wherein OXPAT is highly expressed, Northern blot and immunoblot analyses using RNA and protein isolated from mouse tissues were performed. Interestingly, OXPAT is abundantly expressed in brown adipose tissue (BAT), liver, heart, and soleus, all of which have a high capacity for fatty acid oxidation (Fig. 2*A* and *B*). Expression is lower, but still detectable, in tissues that are relatively less reliant on mitochondrial oxidative metabolism for energy production, including epididymal WAT and more glycolytic skeletal muscles, such as the anterior tibialis and quadriceps. Interestingly, although OXPAT and S3-12 are expressed largely in the same tissues (adipose tissues and striated muscle), the pattern of expression is reciprocal. For example, the OXPAT content of WAT is less than that of BAT, but the opposite is true for S3-12. We have previously shown that contaminating WAT likely accounts for the S3-12 content of BAT depots (10). Similarly, among striated muscles, OXPAT expression is greatest in heart, whereas S3-12 expression is least in heart. OXPAT, but not S3-12, is expressed in liver.

PAT protein expression varies greatly between tissues in mice (Fig. 2). Consistent with previous reports, adipose tissue contains large amounts of perilipin (12). However, here we show that adipose tissue also expresses the other four PAT proteins, with the exception of BAT, which lacks S3-12. Striated muscles, on the other hand, lack perilipin,

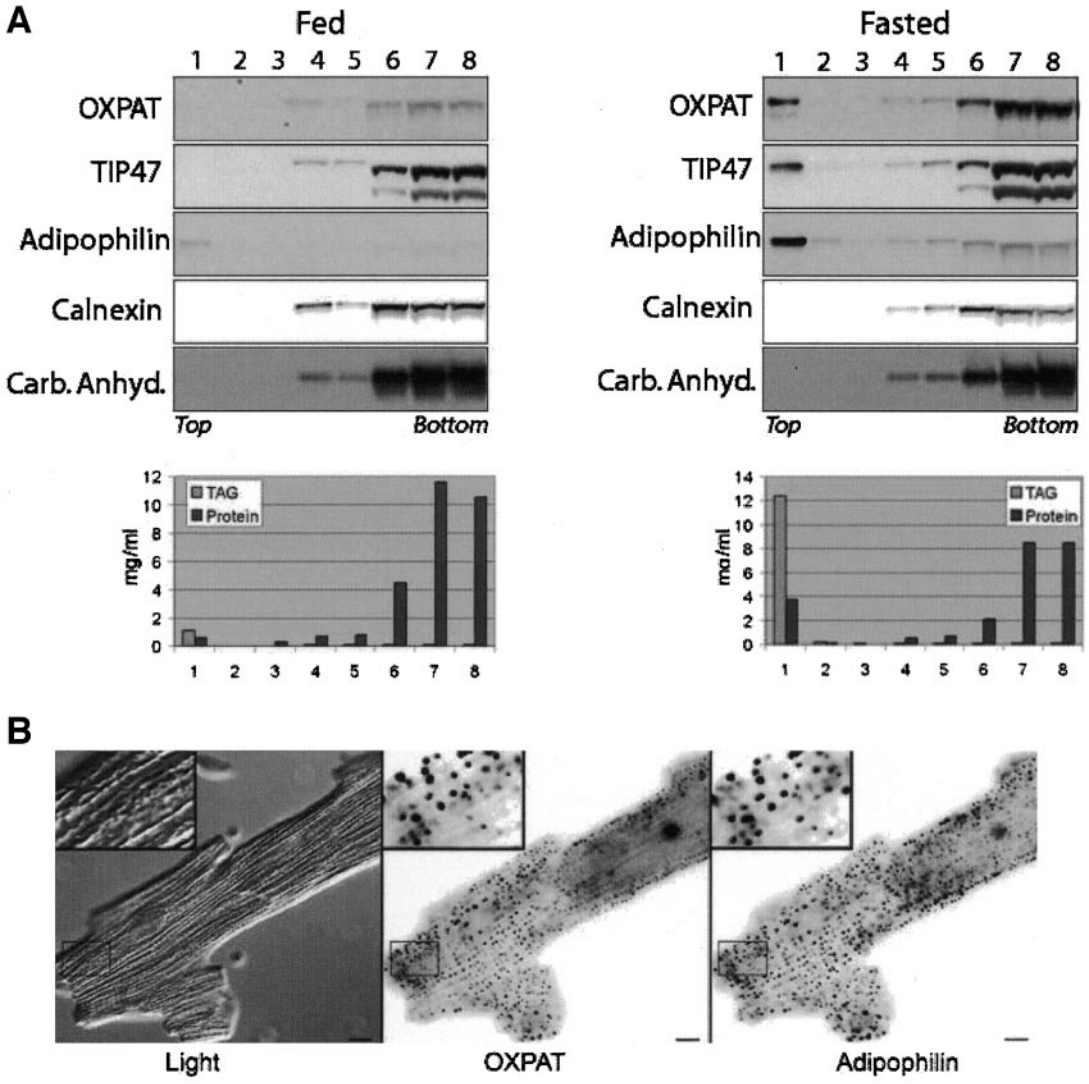

FIG. 3. Analysis of endogenous OXPAT by fractionation of mouse liver and by fluorescence microscopy of adult mouse cardiomyocytes. *A*: Lipid loading of mouse liver by fasting induces OXPAT protein and drives it on to lipid droplets. Liver extracts from fed and fasted mice were fractionated by sucrose density gradient centrifugation. Fractions were immunoblotted and probed with the indicated antibodies (*top panels*) at the following concentrations: α-OXPAT-C 400 ng/ml, α-N-TIP47 400 ng/ml, guinea pig adipophilin antiserum 1:750, 250 ng/ml α-calnexin, and 500 ng/ml a-carbonic anhydrase. Protein and TAG concentration were measured and depicted in the bar graph below the gradients. *B*: OXPAT and the lipid droplet protein adipophilin coat the same structures in adult mouse cardiomyocytes. Cardiomyocytes were stained on coverslips for OXPAT and adipophilin as indicated (α-OXPAT-C at 400 ng/ml; guinea pig adipophilin antiserum 1:500). The light image was produced by differential interference contrast. Bar = 10 μm.

but have the other four PAT proteins, whereas liver has only TIP47, OXPAT, and trace adipophilin.

Endogenous OXPAT coats lipid droplets in fasted mouse liver and in primary mouse cardiomyocytes. We next sought to determine whether OXPAT, like PAT proteins, binds lipid droplets, either constitutively or inducibly. To address this question in a physiological model, we turned to the fasted mouse liver, in which there is significant accumulation of intracellular lipid droplets due to increased delivery of free fatty acids from adipose stores. As expected, fasting significantly increased hepatic TAG content by over 10-fold, as determined biochemically and by steatotic gross appearance of the fasted liver. Livers from chow-fed and fasted mice were analyzed by sucrose density gradient fractionation and immunoblotting (Fig. 3*A*). In the fed liver, OXPAT and TIP47 cofractionated with markers of soluble proteins (carbonic anhydrase) and membrane proteins (calnexin), but neither OXPAT nor TIP47 was detected in the floating (lipid droplet) fraction. Adipophilin, in contrast, was detected only in the lipid droplet fraction of the fed liver. Fasting-induced hepatic TAG accumulation was associated with *1*) increased TAG in the most buoyant (lipid droplet) fraction, *2*) significant induction of OXPAT and adipophilin protein levels, and *3*) enrichment of OXPAT, TIP47, and adipophilin in the lipid droplet fraction. These findings are consistent with our previous report of enrichment of TIP47 and adipophilin in the lipid droplet fraction of oleate-loaded 3T3-L1 adipocytes (18) and with cell fractionation data obtained in COS-7 cells that ectopically express epitope-tagged mouse OXPAT-A (supplemental Figure 4).

To confirm by an independent method that endogenously expressed OXPAT coats lipid droplets, we immunostained isolated adult mouse cardiomyocytes both for OXPAT and for adipophilin, as a marker of lipid droplets (Fig. 3*B*). The antibodies for OXPAT and adipophilin colabeled 1–2 micron punctate structures that aligned in

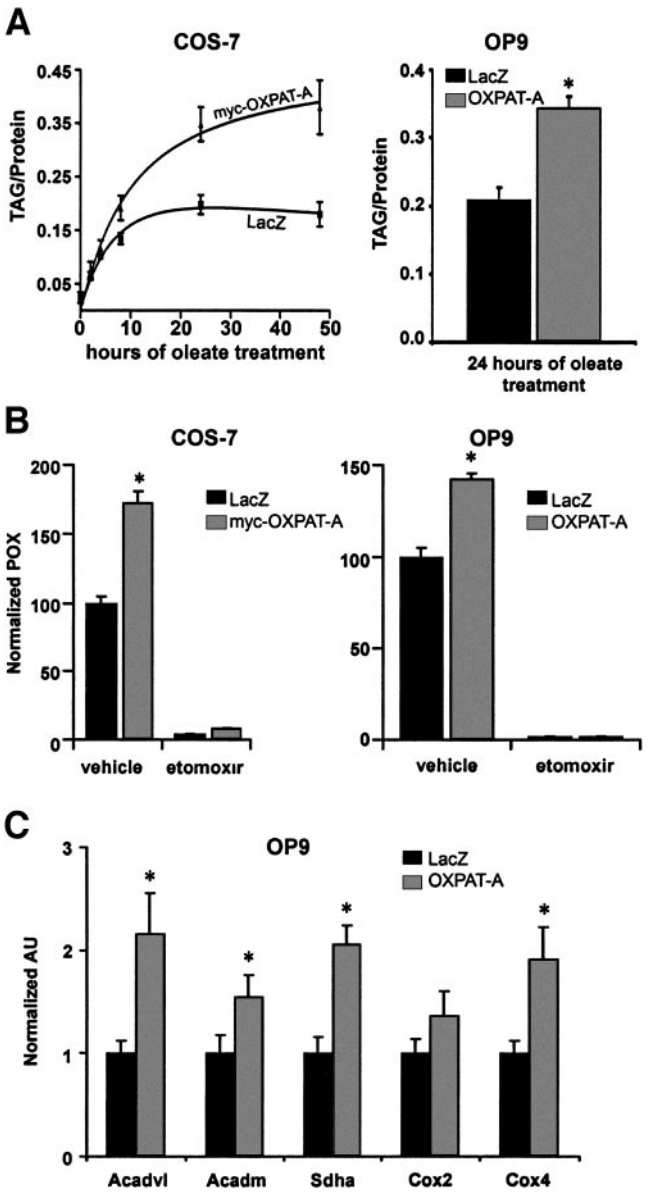

FIG. 4. OXPAT-A increases fatty acid uptake and oxidation. *A*: The left graph depicts mean (± SEM) TAG-to-protein ratios in COS-7 myc-OXPAT-A cells and COS-7 LacZ cells at increasing durations of oleate treatment (n = 9 for each time point). The right bar graph depicts mean (± SEM) TAG-to-protein ratios in OP9 LacZ and OP9 OXPAT-A cells after 24 h of oleate treatment (n = 14). *P < 0.01. *B*: The graphs depict mean (± SEM) rates of palmitate oxidation in COS-7 (left graph) and OP9 (right graph) cells that stably express LacZ or myc-OXPAT-A (COS-7) or OXPAT-A (OP9) in the presence or absence of 50 μmol/l sodium etomoxir. *P < 0.05 vs. LacZ-expressing cells. *C*: Graph depicts mean (± SEM) levels of Acadvl, Acadm, Sdha, COX2, and COX4 mRNA determined by SYBR green RT-PCR (n = 7) using RNA isolated from OP9 cells stably transduced with LacZ or OXPAT-A expression vectors. Values are normalized to LacZ samples (= 1.0) and corrected for 36B4 RNA levels. *P < 0.05 vs. LacZ-expressing cells.

the axis of the myofibers. The adipophilin staining identified these structures as lipid droplets. This punctate lipid droplet staining pattern is similar to that reported for TIP47 and adipophilin in rat soleus muscle (37).

OXPAT-A ectopic expression drives increased rates of TAG accumulation and LCFA oxidation. To investigate the role of OXPAT in cellular lipid metabolism, we generated stable lines of COS-7 cells that express OXPAT-A tagged with an NH_2-terminal myc-epitope (COS-7 myc-OXPAT-A cells) or LacZ (COS-7 LacZ cells), as a control. We first confirmed by cell fractionation and by immunofluorescence microscopy that myc-OXPAT-A inducibly coats lipid droplets upon oleate loading in this heterologous cell system (supplemental Fig. 4). We next asked whether ectopic expression of OXPAT-A increases the cellular capacity to store fatty acid as TAG, as has been shown for perilipin (4) and adipophilin (38,39), by measuring the rates of TAG storage in COS-7 myc-OXPAT-A cells and COS-7 LacZ cells (Fig. 4*A*). Ectopically expressed OXPAT-A in COS-7 cells significantly increased the period in which the initial high rate of TAG accumulation was sustained (Fig. 4*A*). This sustained rapid storage resulted in about twice as much TAG storage by 24 h, as compared with the LacZ control. Similar results were seen in OP9 cells ectopically expressing OXPAT-A (Fig. 4*A*). Interestingly, unlike perilipin (4), OXPAT-A does not increase cellular TAG levels when cells are cultured in normal lean media (Fig. 4*A*, time 0), which suggests that OXPAT-A may provide a less effective barrier to basal lipolysis compared with perilipin.

OXPAT protein is enriched in tissues that rely heavily on oxidation of fatty acids for ATP synthesis. To determine whether constitutive high levels of OXPAT are sufficient to drive fatty acid catabolism, rates of palmitate (C16:0) oxidation were assessed in COS-7 myc-OXPAT-A cells and COS-7 LacZ cells using ^{3}H-palmitic acid. Palmitate oxidation rates were significantly increased in COS-7 myc-OXPAT-A cells compared with COS-7 LacZ cells (Fig. 4*B*). OXPAT-A ectopic expression also increased the rate of palmitate oxidation in OP9 preadipocytes. In both cell types, the OXPAT-mediated increase in LCFA oxidation was abolished by coincubation with sodium etomoxir, which inhibits carnitine palmitoyltransferase 1, the enzyme that catalyzes fatty acid transport into the mitochondrion. These data show that OXPAT-A expression promotes β-oxidation of LCFA and is associated with an increased reliance on LCFA catabolism for energy production.

We next sought to determine whether increased rates of palmitate oxidation were associated with increased expression of genes encoding fatty acid oxidation enzymes, the tricarboxylic acid (TCA) cycle, and oxidative phosphorylation. Real-time quantitative RT-PCR analyses revealed that OXPAT-A ectopic expression increases the expression of genes encoding very-long-chain acyl-CoA dehydrogenase (Acadvl), medium-chain acyl-CoA dehydrogenase (Acadm), subunit a of succinate dehydrogenase (Sdha), and cytochrome C oxidase 4 (Cox4) (Fig. 4*C*). Collectively, these findings suggest that OXPAT-A drives mitochondrial fatty acid oxidation by increasing fatty acid uptake and augmenting expression of enzymes involved in oxidative catabolism.

OXPAT is a PPAR target gene and is induced in liver by fasting and insulin deficiency in a PPARα-dependent manner. Coincident with the identification of OXPAT by a database search as described above, unbiased gene expression microarrays using RNA from mice overexpressing the PPARα in skeletal muscle (MCK-PPARα mice) (21) revealed robust activation of OXPAT gene expression. The PPAR family (α, β, and γ) of nuclear receptor transcription factors controls the expression of multiple genes involved in cellular fatty acid uptake, utilization, and storage (40). Moreover, three members of the PAT family are known targets of the PPAR system (36,41–45). Northern blotting and immunoblotting with cDNA and antibody reagents described above confirm that

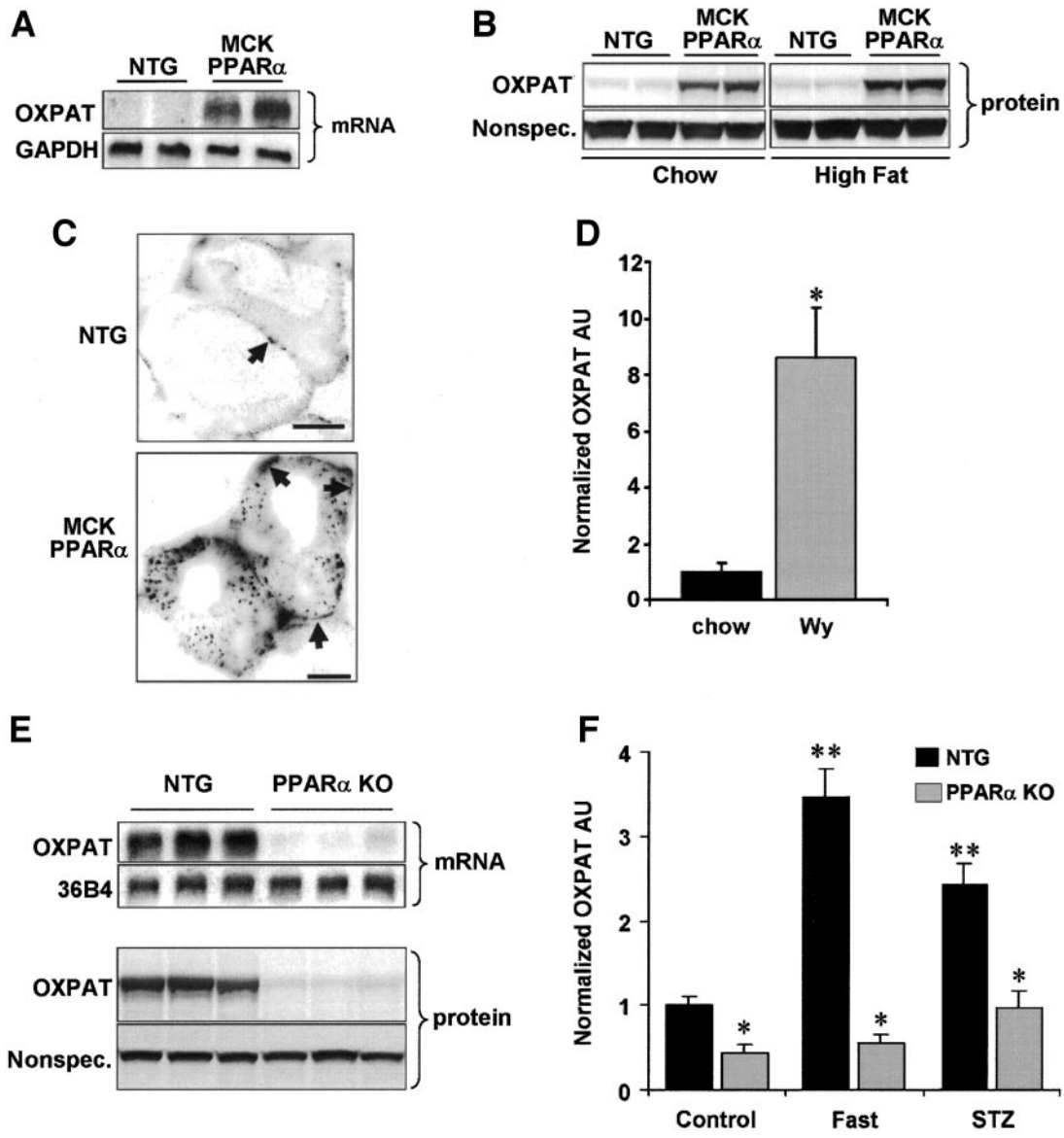

FIG. 5. PPARα controls OXPAT gene expression in striated muscle and liver. Northern blot (*A*) and immunoblot (*B*) depict analyses of RNA or protein isolated from gastrocnemius of MCK-PPARα or nontransgenic (NTG) littermate control mice. Control mice were fed chow. High-fat–fed mice were fed a diet with 43% of its calories from fat. Immunoblot was probed with α-OXPAT-C. *C*: Representative micrographs from high-fat–fed MCK-PPARα mice or NTG littermates. Arrows point to OXPAT staining at the cell cortex. *D*: Mean (± SEM) levels of OXPAT mRNA determined by SYBR green RT-PCR ($n = 6$) using liver RNA isolated from mice given ad libitum access to standard rodent chow (chow) or diet containing 0.1% wt/wt Wy-14643 (Wy). *$P < 0.05$ vs. chow-fed mice. *E*: Representative results of Northern (*top panels*) and immunoblot (*bottom panels*) analyses using cardiac extracts from PPARα KO mice are shown. "Nonspec." labels a nonspecific band from the same lane, demonstrating that similar protein amounts were loaded. *F*: Mean (± SEM) levels of OXPAT mRNA determined by SYBR green RT-PCR ($n = 6$) using RNA isolated from liver of control, fasted, or STZ-treated NTG and PPARα KO mice. *$P < 0.05$ vs. NTG mice in the same treatment group; **$P < 0.05$ vs. NTG control mice.

OXPAT mRNA and protein are increased markedly (~15-fold) in gastrocnemius muscle of MCK-PPARα mice (Fig. 5*A* and *B*) compared with nontransgenic littermate control mice. Gastrocnemius OXPAT protein levels were further increased in MCK-PPARα mice by high-fat feeding, which also modestly increased OXPAT levels in nontransgenic mice (Fig. 5*B*). A similar PPARα-induced increase in OXPAT protein was seen histologically in gastrocnemius muscle of high-fat-fed animals (Fig. 5*C*). Under high-fat conditions in vivo (gastrocnemius of MCK-PPARα mice) and in vitro (COS-7 myc-OXPAT-A cells), OXPAT coats brightly staining puncta that in COS-7 myc-OXPAT-A cells are lipid droplets. Further, in both cell types a small amount of OXPAT is found at the cell cortex (Fig. 5*C* and supplementary Fig. 4*B*). The PPARα-responsiveness of the *Oxpat* gene was also tested in liver. A 1-week course of the PPARα ligand Wy-14643 provided in chow strongly induced hepatic OXPAT gene expression (Fig. 5*D*).

We next took a PPARα loss-of-function (PPARα KO mice) approach to examine PPARα regulation of OXPAT expression. The effect of PPARα deficiency on OXPAT expression was first examined using cardiac RNA and protein since both OXPAT and PPARα are normally expressed at high levels in heart. Northern blotting and immunoblotting analyses demonstrate that myocardial OXPAT levels are markedly diminished in hearts of PPARα KO mice compared with wild-type controls (Fig. 5*E*), indicating that PPARα is required for full expression of OXPAT in heart. Hepatic OXPAT gene expression was significantly increased by fasting and insulin deficiency

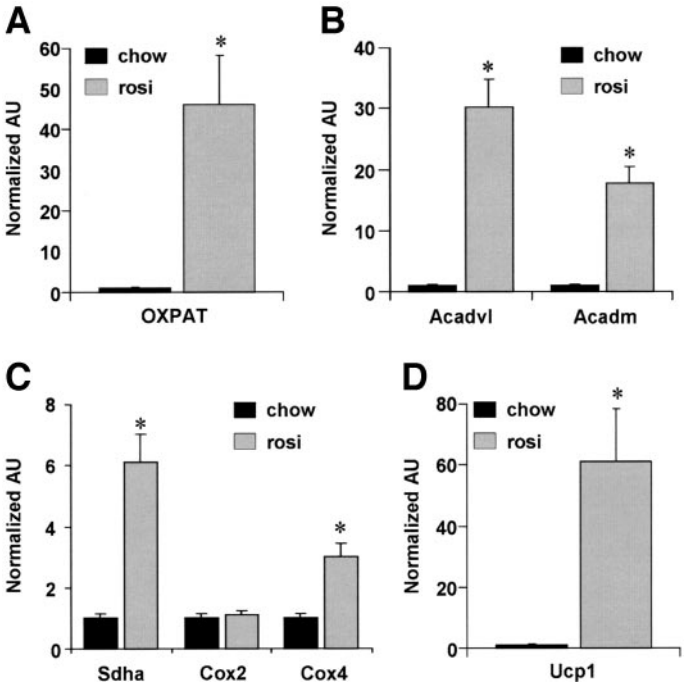

FIG. 6. OXPAT is a PPARγ target gene in mouse WAT. Graphs depict mean (± SEM) levels of OXPAT (*A*); Acadvl and Acadm (*B*); Sdha, Cox2, and Cox4 (*C*); and UCP1 mRNA (*D*) determined by SYBR green RT-PCR ($n = 6$) using epididymal WAT RNA isolated from mice given ad libitum access to standard rodent chow (chow) or chow containing 0.06% wt/wt rosiglitazone (rosi). *$P < 0.05$ vs. chow-fed mice.

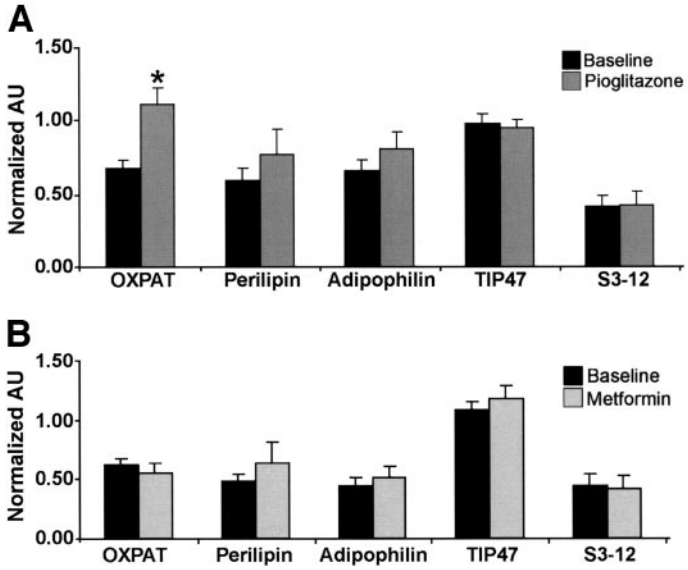

FIG. 7. OXPAT is a PPARγ target in adipose tissue of humans with impaired glucose tolerance. Human subjects with impaired glucose tolerance were randomized to receive either pioglitazone or metformin for 10 weeks. Adipose tissue biopsies were performed and insulin sensitivity was measured before (baseline) and after treatment (pioglitazone or metformin). PAT gene expression before and after pioglitazone ($n = 14$) (*A*) and metformin ($n = 14$) (*B*) treatments is shown. *$P < 0.05$ vs. before treatment.

(Fig. 5*F*), two metabolic states wherein hepatic fatty acid oxidation and the PPARα system are activated (22,46). Interestingly, induction of hepatic OXPAT gene expression in response to fasting and insulin deficiency did not occur in PPARα KO mice (Fig. 5*F*). Thus, PPARα is both sufficient and necessary to activate OXPAT gene expression in striated muscle and liver.

OXPAT is a PPARγ target in WAT. PPARγ is the predominant PPAR isoform in WAT. The thiazolidinediones, a class of insulin-sensitizing drugs, are synthetic agonists for PPARγ and strongly activate PPARγ in adipose tissue (47). Recent evidence suggests that PPARγ agonists also activate oxidative metabolism in white adipose tissue (48,49). OXPAT gene expression in WAT was examined in mice in response to 1 week feeding of the PPARγ agonist, rosiglitazone. As observed in liver with the PPARα agonist, PPARγ activation robustly stimulated OXPAT expression in epididymal WAT (Fig. 6*A*). Coincident with an increase in the expression of OXPAT, rosiglitazone treatment activated expression of several markers of fatty acid oxidation (Acadvl and Acadm), mitochondrial oxidative phosphorylation (Cox4), and the TCA cycle (Sdha). As previously described (49,50), rosiglitazone also increased expression of uncoupling protein 1 (UCP1) in WAT. Collectively, these data indicate that OXPAT expression is activated in WAT coincident with gene markers of increased oxidative catabolism in this storage depot.

PPAR regulation of OXPAT in human adipose tissue. To determine whether the PPAR regulation of OXPAT expression in mouse tissues would translate to human physiology, we measured PAT family mRNA levels in subcutaneous fat and skeletal muscle of humans with impaired glucose tolerance before and after treatment with insulin sensitizers, including the PPARγ agonist pioglitazone. Although pioglitazone treatment did not affect OXPAT expression in skeletal muscle (data not shown), it did lead to a significant increase in OXPAT mRNA in subcutaneous fat (Fig. 7). Metformin treatment was not associated with changes in OXPAT expression in adipose tissue or skeletal muscle. Other PAT family mRNAs were not induced significantly in adipose or muscle by either insulin sensitizer, though there was a trend toward increased perilipin expression in adipose tissue with pioglitazone. That OXPAT expression was increased with pioglitazone but not metformin treatment suggests that the result was likely a direct effect of PPARγ activation in adipocytes.

Because OXPAT RNA was increased by pioglitazone, we hypothesized that OXPAT expression might correlate with obesity and insulin resistance in a larger population. To test this hypothesis, we measured OXPAT gene expression in subcutaneous adipose tissue of 85 nondiabetic subjects with a wide range of obesity and insulin sensitivity (S_I) (Fig. 8). There was a significant negative correlation between OXPAT expression and BMI in subcutaneous adipose tissue ($r = -0.32$, $P < 0.003$) and a significant positive correlation between OXPAT expression and S_I ($r = 0.28$, $P < 0.002$). BMI is significantly inversely related to S_I, and hence we used partial correlation coefficients to separate the independent effects of BMI and S_I. Whereas the correlation between adipose OXPAT expression and BMI remained significant when controlled for S_I ($r = -0.27$, $P < 0.02$), the correlation between adipose OXPAT expression and S_I did not remain significant when controlled for BMI ($r = 0.07$, $P < 0.58$). These data suggest that OXPAT expression in subcutaneous adipose tissue is decreased with obesity and, moreover, that the decrease in OXPAT with insulin resistance is driven predominantly by the association between obesity and insulin resistance.

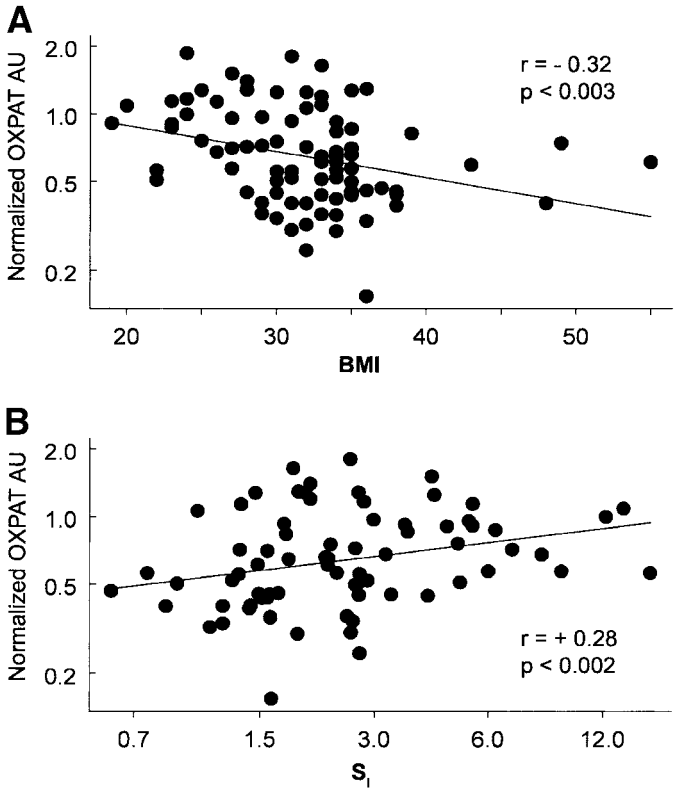

FIG. 8. OXPAT gene expression negatively correlates with BMI in nondiabetic human subjects. OXPAT adipose tissue expression was measured in the fasting state of human subjects covering a range of BMI ($n = 85$) and S_I ($n = 74$). The natural log of OXPAT was plotted against BMI ($r = -0.32$, $P < 0.003$) (*A*) and the natural log of S_I ($r = +0.28$, $P < 0.002$) (*B*).

DISCUSSION

Four members of the PAT family have been shown to bind lipid droplets. We have begun to characterize the fifth member in this family, OXPAT. We have shown that, as with other PAT proteins, OXPAT can bind to lipid droplets and promote LCFA-induced TAG accumulation. OXPAT also increases oxidation of LCFA. Consistent with these data, OXPAT mRNA and protein are most highly expressed in mouse tissues that have large capacities for fatty acid oxidation. In these tissues, OXPAT expression is induced by physiologic, pharmacologic, and genetic perturbations that increase utilization of fatty acids for oxidative phosphorylation. Hepatic OXPAT is induced significantly during fasting, and a significant subset of OXPAT redistributes to lipid droplets in response to the increased lipid flux induced by fasting. In liver and striated muscle, PPARα activation is both necessary and sufficient to drive increased OXPAT gene expression. Treatment of both mice and humans with PPARγ agonists also increased OXPAT gene expression in adipose tissue. Multiple complete mammalian genomes have been sequenced, and no other sequence that is obviously similar to the PAT genes has been identified. This suggests that OXPAT likely completes the mammalian PAT family.

The *Oxpat* gene is located immediately upstream of the gene that encodes S3-12 and is in close proximity to the gene for TIP47 on mouse chromosome 17. These physical relationships between the three genes are conserved on human chromosome 19. Thus, it is likely that one or more of these genes arose by gene duplication. TIP47 is most likely the primordial gene, because its expression in tissues is ubiquitous, as opposed to the much more restricted expression of OXPAT and S3-12 in tissues that use fatty acids as an energy source or an energy depot. Our data suggest that OXPAT and S3-12 gene expression is coordinately and reciprocally regulated. Coordinate expression is revealed by the significant overlap in tissues that express both genes. There is an additional level of reciprocal regulation, however, that results in relatively greater OXPAT expression in tissues with higher oxidative metabolic capacity (BAT, heart, soleus) and greater S3-12 expression in WAT, which is specialized for lipid storage. This observation suggests that the functions of these two exchangeable lipid droplet proteins may be reciprocal as well, with OXPAT packaging TAG that is available for hydrolysis and subsequent oxidation, and S3-12 packaging TAG that is destined for storage. Recently, Larigauderie et al. (39) have suggested that adipophilin increases TAG in human macrophages by both stimulating TAG synthesis and by inhibiting β-oxidation. Thus, a possible mechanism by which OXPAT increases LCFA oxidation is by displacing an inhibitor of β-oxidation, adipophilin, from the lipid droplet coat. Notably, all three PAT proteins encoded by genes on mouse chromosome 17 associate with the surface of lipid droplets in an inducible and reversible manner, as opposed to the constitutive lipid droplet association observed for the other PAT proteins, adipophilin and perilipin.

Concomitant with our database discovery of the gene encoding OXPAT, unbiased gene expression array profiling of transgenic mice suggested that OXPAT was a target gene of PPARα. The PPAR family of ligand-activated, nuclear receptor transcription factors controls the expression of nearly every step in the cellular fatty acid uptake, oxidation, and storage pathways (51). Recent work has demonstrated that the other members of the PAT family, with the exception of TIP47, are induced in response to PPARγ ligand administration (36,41,43) in mice. Adipophilin expression is induced in liver of PPARα agonist–treated mice (45). Several lines of evidence presented herein indicate that OXPAT is also a bona fide PPAR target gene. First, OXPAT expression was robustly induced by PPARα overexpression, PPARα-specific ligand administration, and physiologic conditions known to activate PPARα (fasting and insulin deficiency). Secondly, PPARγ ligands activate OXPAT expression in human and mouse WAT, a tissue enriched in PPARγ. Finally, PPARα KO mice exhibit markedly diminished hepatic and cardiac expression of OXPAT at baseline and are refractory to the induction of OXPAT expression in liver by fasting and insulin deficiency. These latter findings place OXPAT in the class of PPARα target genes, including acyl-CoA oxidase (Acox1) and Acadm, that require PPARα for full induction by fasting (22). This requirement contrasts with other PPARα target genes, including adipophilin (45) and Cpt1a (22), that are induced robustly during fasting in liver of PPARα KO mice. Interestingly, we also show that OXPAT overexpression activates expression of other known PPAR target genes involved in mitochondrial fatty acid oxidation and oxidative metabolism in OP9 cells. This suggests that OXPAT may drive import of fatty acids that act as PPAR ligands and potentially places OXPAT both upstream and downstream of PPARα in this gene-regulatory cascade. The activation of OXPAT by fasting and insulin deficiency may provide a 'feed-forward' mechanism to boost fatty acid oxidation capacity and catabolize excess fatty acids under physiologic and pathophysiologic conditions.

Some of the findings from the mouse and cell culture experiments were replicated in the more heterogeneous human subjects. In mice and humans, TZD treatment increased adipose OXPAT expression, though the effect was more modest in humans. Such an effect in human adipose would be predicted to have a favorable effect on adiposity by promoting oxidative lipid metabolic pathways. We observed a negative correlation between expression of OXPAT in human subcutaneous adipose tissue and BMI. Our data do not indicate whether OXPAT expression is a determinant of human adiposity or is determined by it. Microarray studies have suggested that genes involved in oxidative phosphorylation pathways in muscle of diabetic/insulin-resistant humans are downregulated (52,53). Thus, the reduction in adipose OXPAT expression that we have observed with increasing BMI may reflect a more generalized effect on a coordinately regulated set of genes. Alternatively, our in vitro and in vivo data that are consistent with OXPAT being both upstream and downstream of PPAR activation suggest the possibility that OXPAT itself may influence adiposity. Gain- and loss-of-function experiments in mice will be helpful in addressing this and other questions.

Recently, Yamaguchi et al. (54) published findings that myocardial lipid droplet protein (MLDP), a protein identical in amino acid sequence to OXPAT-B, is a lipid droplet protein regulated by PPARα and induced by fasting in heart and liver. These findings are consistent with our data, although we also demonstrate significant OXPAT protein expression in BAT, liver, and oxidative versus glycolytic muscles. Also, whereas MLDP was not thought to be PPARγ regulated, we have found that PPARγ agonists induce OXPAT gene expression in mouse and human adipose tissue.

Our data collectively suggest that OXPAT is a marker of a favorable metabolic adaptation to increased fatty acid availability in the adipose tissue of lean healthy individuals. Whether this adaptation represents preferential delivery of cellular lipid for oxidation, as suggested by the in vitro studies, or other favorable adaptations remains for future investigations. It has been proposed that obese humans exhibit "metabolic inflexibility" with regard to oxidative fuel selection in skeletal muscle (55). According to this model, during fasting lipid oxidation does not appropriately increase in skeletal muscle, which leads in turn to increased intramyocellular lipid. Increased muscle lipid may then provide substrates that negatively influence insulin signaling pathways, thereby leading to insulin resistance (56). We have shown that OXPAT is a fasting- and PPAR-induced, exchangeable lipid droplet protein that can promote LCFA esterification into TAG and LCFA oxidation. As such, OXPAT may be important for maintaining flexible metabolic fuel selection, and its downregulation in obesity may contribute to loss of this adaptive response.

ACKNOWLEDGMENTS

This work was supported by National Institutes of Health grants RO1 DK068046 (P.E.B.); KO1 DK062903 (B.N.F.); T32 DK07296 (N.E.W.); P30 DK52574 (Histology Core of the Digestive Diseases Research Cores Center); DK 39176 and DK 71277 (P.A.K.); a Merit Review Grant from the Veterans Administration (P.A.K.); and M01RR14288 of the General Clinical Research Center (P.A.K.).

We thank the Developmental Studies Hybridoma Bank at the University of Iowa, Iowa City, Iowa, for providing antibodies used in this study.

The authors thank Horace J. Spencer, III, for statistical assistance; Ilya Treskov and Anthony Muslin for their generous gift of adult mouse cardiomyocytes; and Michelle Mo, Dan Delitto, and Bounleut Phanavanh for expert laboratory technical assistance.

REFERENCES

1. Miura S, Gan JW, Brzostowski J, Parisi MJ, Schultz CJ, Londos C, Oliver B, Kimmel AR: Functional conservation for lipid storage droplet association among Perilipin, ADRP, and TIP47 (PAT)-related proteins in mammals, *Drosophila*, and *Dictyostelium*. *J Biol Chem* 277:32253–32257, 2002
2. Tansey JT, Sztalryd C, Hlavin EM, Kimmel AR, Londos C: The central role of perilipin a in lipid metabolism and adipocyte lipolysis. *IUBMB Life* 56:379–385, 2004
3. Londos C, Sztalryd C, Tansey JT, Kimmel AR: Role of PAT proteins in lipid metabolism. *Biochimie* 87:45–49, 2005
4. Brasaemle DL, Rubin B, Harten IA, Gruia-Gray J, Kimmel AR, Londos C: Perilipin A increases triacylglycerol storage by decreasing the rate of triacylglycerol hydrolysis. *J Biol Chem* 275:38486–38493, 2000
5. Sztalryd C, Xu G, Dorward H, Tansey JT, Contreras JA, Kimmel AR, Londos C: Perilipin A is essential for the translocation of hormone-sensitive lipase during lipolytic activation. *J Cell Biol* 161:1093–1103, 2003
6. Chang BH, Li L, Paul A, Taniguchi S, Nannegari V, Heird WC, Chan L: Protection against fatty liver but normal adipogenesis in mice lacking adipose differentiation-related protein. *Mol Cell Biol* 26:1063–1076, 2006
7. Tansey JT, Sztalryd C, Gruia-Gray J, Roush DL, Zee JV, Gavrilova O, Reitman ML, Deng CX, Li C, Kimmel AR, Londos C: Perilipin ablation results in a lean mouse with aberrant adipocyte lipolysis, enhanced leptin production, and resistance to diet-induced obesity. *Proc Natl Acad Sci U S A* 98:6494–6499, 2001
8. Martinez-Botas J, Anderson JB, Tessier D, Lapillonne A, Chang BH, Quast MJ, Gorenstein D, Chen KH, Chan L: Absence of perilipin results in leanness and reverses obesity in Lepr(db/db) mice. *Nat Genet* 26:474–479, 2000
9. Wolins NE, Rubin B, Brasaemle DL: TIP47 associates with lipid droplets. *J Biol Chem* 276:5101–5108, 2001
10. Wolins NE, Skinner JR, Schoenfish MJ, Tzekov A, Bensch KG, Bickel PE: Adipocyte protein S3-12 coats nascent lipid droplets. *J Biol Chem* 278: 37713–37721, 2003
11. Brasaemle DL, Barber T, Wolins NE, Serrero G, Blanchette-Mackie EJ, Londos C: Adipose differentiation-related protein is an ubiquitously expressed lipid storage droplet-associated protein. *J Lipid Res* 38:2249–2263, 1997
12. Greenberg AS, Egan JJ, Wek SA, Garty NB, Blanchette-Mackie EJ, Londos C: Perilipin, a major hormonally regulated adipocyte-specific phosphoprotein associated with the periphery of lipid storage droplets. *J Biol Chem* 266:11341–11346, 1991
13. Greenberg AS, Egan JJ, Wek SA, Moos MC Jr, Londos C, Kimmel AR: Isolation of cDNAs for perilipins A and B: sequence and expression of lipid droplet-associated proteins of adipocytes. *Proc Natl Acad Sci U S A* 90:12035–12039, 1993
14. Brasaemle DL, Barber T, Kimmel AR, Londos C: Post-translational regulation of perilipin expression: stabilization by stored intracellular neutral lipids. *J Biol Chem* 272:9378–9387, 1997
15. Diaz E, Pfeffer SR: TIP47: a cargo selection device for mannose 6-phosphate receptor trafficking. *Cell* 93:433–443, 1998
16. Xu G, Sztalryd C, Lu X, Tansey JT, Gan J, Dorward H, Kimmel AR, Londos C: Post-translational regulation of adipose differentiation-related protein by the ubiquitin/proteasome pathway. *J Biol Chem* 280:42841–42847, 2005
17. Xu G, Sztalryd C, Londos C: Degradation of perilipin is mediated through ubiquitination-proteasome pathway. *Biochim Biophys Acta* 1761:83–90, 2006
18. Wolins NE, Quaynor BK, Skinner JR, Schoenfish MJ, Tzekov A, Bickel PE: S3-12, Adipophilin, and TIP47 package lipid in adipocytes. *J Biol Chem* 280:19146–19155, 2005
19. Benson DA, Karsch-Mizrachi I, Lipman DJ, Ostell J, Wheeler DL: GenBank. *Nucleic Acid Res* 34 (Database issue):D16–D20, 2006
20. Lee SS, Pineau T, Drago J, Lee EJ, Owens JW, Kroetz DL, Fernandez-Salguero PM, Westphal H, Gonzalez FJ: Targeted disruption of the alpha isoform of the peroxisome proliferator-activated receptor gene in mice results in abolishment of the pleiotropic effects of peroxisome proliferators. *Mol Cell Biol* 15:3012–3022, 1995
21. Finck BN, Bernal-Mizrachi C, Han DH, Coleman T, Sambandam N,

LaRiviere LL, Holloszy JO, Semenkovich CF, Kelly DP: A potential link between muscle peroxisome proliferator- activated receptor-alpha signaling and obesity-related diabetes. *Cell Metab* 1:133–144, 2005
22. Leone TC, Weinheimer CJ, Kelly DP: A critical role for the peroxisome proliferator-activated receptor alpha (PPARalpha) in the cellular fasting response: the PPARalpha-null mouse as a model of fatty acid oxidation disorders. *Proc Natl Acad Sci U S A* 96:7473–7478, 1999
23. Kelly DP, Gordon JI, Alpers R, Strauss AW: The tissue-specific expression and developmental regulation of two nuclear genes encoding rat mitochondrial proteins: medium chain acyl-CoA dehydrogenase and mitochondrial malate dehydrogenase. *J Biol Chem* 264:18921–18925, 1989
24. Brasaemle DL, Dolios G, Shapiro L, Wang R: Proteomic analysis of proteins associated with lipid droplets of basal and lipolytically stimulated 3T3–L1 adipocytes. *J Biol Chem* 279:46835–46842, 2004
25. Wolins NE, Quaynor BK, Skinner JR, Tzekov A, Park C, Choi K, Bickel PE: OP9 mouse stromal cells rapidly differentiate into adipocytes: characterization of a useful new model of adipogenesis. *J Lipid Res* 47:450–460, 2006
26. Ory DS, Neugeboren BA, Mulligan RC: A stable human-derived packaging cell line for production of high titer retrovirus/vesicular stomatitis virus G pseudotypes. *Proc Natl Acad Sci U S A* 93:11400–11406, 1996
27. DeBosch B, Treskov I, Lupu TS, Weinheimer C, Kovacs A, Courtois M, Muslin AJ: Akt1 is required for physiological cardiac growth. *Circulation* 113:2097–2104, 2006
28. Djouadi F, Bonnefont JP, Munnich A, Bastin J: Characterization of fatty acid oxidation in human muscle mitochondria and myoblasts. *Mol Genet Metab* 78:112–118, 2003
29. Rasouli N, Raue U, Miles LM, Lu T, Di Gregorio GB, Elbein SC, Kern PA: Pioglitazone improves insulin sensitivity through reduction in muscle lipid and redistribution of lipid into adipose tissue. *Am J Physiol Endocrinol Metab* 288:E930–E934, 2005
30. Bergman RN, Prager R, Volund A, Olefsky JM: Equivalence of the insulin sensitivity index in man derived by the minimal model method and the euglycemic glucose clamp. *J Clin Invest* 79:790–800, 1987
31. Boston RC, Stefanovski D, Moate PJ, Sumner AE, Watanabe RM, Bergman RN: MINIMOD Millennium: a computer program to calculate glucose effectiveness and insulin sensitivity from the frequently sampled intravenous glucose tolerance test. *Diabetes Techno Ther* 5:1003–1015, 2003
32. Di Gregorio GB, Yao-Borengasser A, Rasouli N, Varma V, Lu T, Miles LM, Ranganathan G, Peterson CA, McGehee RE, Kern PA: Expression of CD68 and macrophage chemoattractant protein-1 genes in human adipose and muscle tissues: association with cytokine expression, insulin resistance, and reduction by pioglitazone. *Diabetes* 54:2305–2313, 2005
33. Nair R, Rost B: Mimicking cellular sorting improves prediction of subcellular localization. *J Mol Biol* 348:85–100, 2005
34. Bendtsen JD, Nielsen H, von Heijne G, Brunak S: Improved prediction of signal peptides: SignalP 3.0. *J Mol Biol* 340:783–795, 2004
35. Bateman A, Coin L, Durbin R, Finn RD, Hollich V, Griffiths-Jones S, Khanna A, Marshall M, Moxon S, Sonnhammer EL, Studholme DJ, Yeats C, Eddy SR: The Pfam protein families database. *Nucleic Acid Res* 32:D138–D141, 2004
36. Dalen KT, Schoonjans K, Ulven SM, Weedon-Fekjaer MS, Bentzen TG, Koutnikova H, Auwerx J, Nebb HI: Adipose tissue expression of the lipid droplet-associating proteins S3-12 and perilipin is controlled by peroxisome proliferator-activated receptor-γ. *Diabetes* 53:1243–1252, 2004
37. Prats C, Donsmark M, Qvortrup K, Londos C, Sztalryd C, Holm C, Galbo H, Ploug T: Decrease in intramuscular lipid droplets and translocation of hormone-sensitive lipase in response to muscle contraction and epinephrine. *J Lipid Res*. In press
38. Imamura M, Inoguchi T, Ikuyama S, Taniguchi S, Kobayashi K, Nakashima N, Nawata H: ADRP stimulates lipid accumulation and lipid droplet formation in murine fibroblasts. *Am J Physiol Endocrinol Metab* 283: E775–E783, 2002
39. Larigauderie G, Cuaz-Perolin C, Younes AB, Furman C, Lasselin C, Copin C, Jaye M, Fruchart JC, Rouis M: Adipophilin increases triglyceride storage in human macrophages by stimulation of biosynthesis and inhibition of beta-oxidation. *FEBS J* 273:3498–3510, 2006
40. Desvergne B, Wahli W: Peroxisome proliferator-activated receptors: nuclear control of metabolism. *Endocr Rev* 20:649–688, 1999
41. Nagai S, Shimizu C, Umetsu M, Taniguchi S, Endo M, Miyoshi H, Yoshioka N, Kubo M, Koike T: Identification of a functional peroxisome proliferator-activated receptor responsive element within the murine perilipin gene. *Endocrinology* 145:2346–2356, 2004
42. Shimizu M, Takeshita A, Tsukamoto T, Gonzalez FJ, Osumi T: Tissue-selective, bidirectional regulation of PEX11 alpha and perilipin genes through a common peroxisome proliferator response element. *Mol Cell Biol* 24:1313–1323, 2004
43. Arimura N, Horiba T, Imagawa M, Shimizu M, Sato R: The peroxisome proliferator-activated receptor gamma regulates expression of the perilipin gene in adipocytes. *J Biol Chem* 279:10070–10076, 2004
44. Tobin KA, Harsem NK, Dalen KT, Staff AC, Nebb HI, Duttaroy AK: Regulation of ADRP expression by long-chain polyunsaturated fatty acids in BeWo cells, a human placental choriocarcinoma cell line. *J Lipid Res* 47:815–823, 2006
45. Dalen KT, Ulven SM, Arntsen BM, Solaas K, Nebb HI: PPARalpha activators and fasting induce the expression of adipose differentiation-related protein in liver. *J Lipid Res* 47:931–943, 2006
46. Kroetz DL, Yook P, Costet P, Bianchi P, Pineau T: Peroxisome proliferator-activated receptor alpha controls the hepatic CYP4A induction adaptive response to starvation and diabetes. *J Biol Chem* 273:31581–31589, 1998
47. Spiegelman BM: PPAR-γ: adipogenic regulator and thiazolidinedione receptor. *Diabetes* 47:507–514, 1998
48. Bogacka I, Ukropcova B, McNeil M, Gimble JM, Smith SR: Structural and functional consequences of mitochondrial biogenesis in human adipocytes in vitro. *J Clin Endocrinol Metab* 90:6650–6656, 2005
49. Bogacka I, Xie H, Bray GA, Smith SR: Pioglitazone induces mitochondrial biogenesis in human subcutaneous adipose tissue in vivo. *Diabetes* 54: 1392–1399, 2005
50. Wilson-Fritch L, Nicoloro S, Chouinard M, Lazar MA, Chui PC, Leszyk J, Straubhaar J, Czech MP, Corvera S: Mitochondrial remodeling in adipose tissue associated with obesity and treatment with rosiglitazone. *J Clin Invest* 114:1281–1289, 2004
51. Feige JN, Gelman L, Michalik L, Desvergne B, Wahli W: From molecular action to physiological outputs: peroxisome proliferator-activated receptors are nuclear receptors at the crossroads of key cellular functions. *Prog Lipid Res* 45:120–159, 2006
52. Mootha VK, Lindgren CM, Eriksson KF, Subramanian A, Sihag S, Lehar J, Puigserver P, Carlsson E, Ridderstrale M, Laurila E, Houstis N, Daly MJ, Patterson N, Mesirov JP, Golub TR, Tamayo P, Spiegelman B, Lander ES, Hirschhorn JN, Altshuler D, Groop LC: PGC-1alpha-responsive genes involved in oxidative phosphorylation are coordinately downregulated in human diabetes. *Nat Genet* 34:267–273, 2003
53. Patti ME, Butte AJ, Crunkhorn S, Cusi K, Berria R, Kashyap S, Miyazaki Y, Kohane I, Costello M, Saccone R, Landaker EJ, Goldfine AB, Mun E, DeFronzo R, Finlayson J, Kahn CR, Mandarino LJ: Coordinated reduction of genes of oxidative metabolism in humans with insulin resistance and diabetes: potential role of PGC1 and NRF1. *Proc Natl Acad Sci U S A* 100:8466–8471, 2003
54. Yamaguchi T, Matsushita S, Motojima K, Hirose F, Osumi T: MLDP, a novel PAT family protein localized to lipid droplets and enriched in the heart, is regulated by peroxisome proliferator-activated receptor alpha. *J Biol Chem* 281:14232–14240, 2006
55. Kelley DE, Mandarino LJ: Fuel selection in human skeletal muscle in insulin resistance: a reexamination. *Diabetes* 49:677–683, 2000
56. Shulman GI: Cellular mechanisms of insulin resistance. *J Clin Invest* 106:171–176, 2000